CHINESE JOURNAL OF PHYSICS VOL. 43, NO. 3-I JUNE 2005

Horizontal Wavelength of Gravity Waves in the Lower Atmosphere Measured by the SOUSY Svalbard Radar

F. S. Kuo[1] and Jürgen Röttger[2]

[1] *Department of Electro-Optical Engineering, Van Nung University, Chung-Li, Taiwan*
[2] *Max-Planck-Institut, Katlenburg-Lindau, Germany*

(Received October 6, 2004)

Height profiles of the vertical atmospheric motion are analyzed to obtain the vertical phase and group velocities of the atmospheric gravity wave motion by the technique of phase and group velocity tracing. Then the horizontal wave vector component along the direction of the mean wind is obtained by the gravity wave dispersion relation, and the angle $|\theta|$ between the horizontal wave vector and the mean wind velocity is obtained by the polarization relation. The data were taken during the period between March 30 and April 24 in 2000 using the SOUSY Svalbard Radar. The altitude range of measurement is between 2.4 km and 14.25 km. Most of the wave packets (about 75%) in the Range-Time-Intensity (RTI) plots of velocity show that the vertical phase and group velocities are in the opposite direction (Type 1 wave packets). The rest (about 25%) are shorter lasting wave packets showing that the vertical phase and group velocities are in the same direction (Type 2 wave packets). By horizontal wave vector analysis we have found no wave packet moving against the background wind. Statistical analysis of the angle $|\theta|$, which is the angle between the horizontal wave vector and the background wind velocity vector, reveals a trend, namely that the percentage of wave packets monotonically decreases with the angle $|\theta|$.

PACS numbers: 92.60.Dj, 94.20.Bb

I. INTRODUCTION

Very-High-Frequency Mesosphere-Stratosphere-Troposphere radars (VHF MST radars) have been intensively used for the study of atmospheric dynamics. They are particularly useful for observations of atmospheric gravity waves, which were shown in some of the early radar experiments [1–4]. Such case studies, as well as extensive statistical analyses, have proven essential for understanding the properties of these waves, such as their spectra [5] and their momentum deposition into the mean wind [6–8]. Gravity wave features were measured with radar, rocket, and satellite during the CADRE/MALTED campaign at equatorial latitudes in Peru [9, 10]. These latter radar observations were done so far in the middle and lower latitudes, but there had also been a few analyses of high polar latitude of gravity waves observed by radar [11] and detected in operational radiosonde data [12]. These observations were in the troposphere, stratosphere, and mesosphere. In this paper we investigate MST VHF radar observations of gravity waves in the troposphere and lower stratosphere at high polar latitudes which were done with the SOUSY Svalbard Radar [13].

Atmospheric gravity waves in the linear regime are characterized by a special relation

between their vertical phase velocity and group velocity, namely, the direction of the vertical phase velocity is not in the same direction as its group velocity. Traditionally one tends to apply this principle to suggest that the energy source of an atmospheric gravity wave can be identified from its phase velocity [14]. However, it is also known that when the horizontal phase velocity component along the mean wind velocity is smaller than, and in the same direction as the background wind velocity, its vertical phase velocity will reverse to propagate in the same direction as the vertical group velocity (known as the Doppler shift effect). Therefore, the direction of the vertical phase velocity does not immediately imply accurate information on the wave's energy source. Direct measurement of the vertical group velocity is therefore required to gain information on the energy transport by gravity waves in the atmosphere. A new method called phase and group velocity tracing was developed [15] to measure the vertical phase and group velocities.

In developing the technique of phase and group velocity tracing [15], it was shown by numerical simulation that any single wave packet propagation could be unambiguously identified. But the real data is not as homogeneous (i.e., not usually a wave packet of limited bandwidth) as the data generated by the controlled numerical simulation, because both energy-upward-propagating and energy-downward-propagating waves with same wave frequency may be created simultaneously in the same place, and the superposition between them causes difficulty in identification. Therefore, we must separate the upward propagating waves from the downward propagating waves. A proper procedure of separation becomes a key to such a study. This technique of velocity tracing was then applied to analyze the data observed by the SOUSY-Svabard Radar in October–2000 in the altitude range between 2.4 km and 17.4 km [16], in which hundreds of wave packets were identified from Range-Time-Intensity (RTI) plots of velocities, and two types of wave packets with characteristic wave periods in the range 15–45 minutes were found: About 85% of the wave packets show that the vertical phase and group velocities are in opposite direction (which we call Type 1 wave packets), revealing the typical characteristics of the propagation of atmospheric gravity waves in the linear regime; about 15% of the wave packets show that their vertical phase and group velocities are in the same direction (Type 2 wave packets). It was also demonstrated that, when the vertical components of the phase and group velocities of a gravity wave packet are obtained and reveal the characteristics of gravity waves in the linear regime, one may go on to estimate the corresponding horizontal wavelength along the direction of the background wind velocity from the dispersion relation.

We will move one step further in this paper. With the simultaneous information on the background wind velocity available (through the five beam directions the radar measures the mean horizontal background wind velocity as well), we will not only calculate the horizontal wave-number component of a wave packet along the direction of the background wind velocity, but also will deduce the angle between the horizontal wave vector and its background wind velocity by the gravity wave polarization equation. This analysis will enable the presentation of complete wave packet information, including its characteristic wave period and three-dimensional wave vector, from the observations of just one single radar site.

II. RADAR OBSERVATIONS

VHF radars are very proper tools for gravity wave observations, since they allow height and time resolutions adapted to gravity wave parameters. One of these radars is the SOUSY Svalbard Radar (SSR), which is applied to mesosphere, stratosphere, and troposphere studies in the high Arctic region at 78 degrees N and 16 degrees E on the archipelago of Svalbard [13]. This MST radar is operated in the VHF band at 53.5 MHz with a peak power of 70 kW and has a phased-antenna array consisting of 356 Yagis yielding a gain of 33 dBi and 4 degrees half-power beam width. In this experiment we have measured the horizontal wind velocity using obliquely pointing beams, which are pointed cyclically 5 degrees from the vertical direction to the east, north, west, and south. In each cycle, the zonal and meridional velocities are obtained by averaging over the four oblique measurements, corresponding approximately to a measurement at the symmetric center of these four points at each height. Therefore, the data set consist of zonal and meridional wind velocities every 2.44 minutes along the vertical direction from the altitude of 2.4 km to 14.25 km with a height resolution of 150 meters.

III. METHOD OF ANALYSIS

III-1. Separation of upward waves and downward waves

Consider a vertical velocity oscillation profile of the atmospheric motion $\psi(z,t)$ as a function of height z and time t. First we make a finite Fourier transformation of $\psi(z,t)$ over the height coordinate z at each fixed time t to obtain the coefficients $A_n(t)$ and $B_n(t)$ of the function $\cos(nz)$ and the function $\sin(nz)$, respectively:

$$\psi(z,t) = \sum_n \{A_n(t)\cos(nz) + B_n(t)\sin(nz)\}\,. \tag{1}$$

Then, finite Fourier transformations are made on each $A_n(t)$ and $B_n(t)$ over time t:

$$A_n(t) = \sum_\sigma \{A_{n\sigma}^{(1)}\cos(\sigma t) + B_{n\sigma}^{(1)}\sin(\sigma t)\}\,, \tag{2a}$$

$$B_n(t) = \sum_\sigma \{A_{n\sigma}^{(2)}\cos(\sigma t) + B_{n\sigma}^{(2)}\sin(\sigma t)\}\,, \tag{2b}$$

where n and σ represent the vertical wave-number and the observed frequency of the component wave, respectively. Substituting (2a) and (2b) back into (1) with some algebra manipulations, we obtain

$$\begin{aligned}\psi(z,t) = &\sum_{n,\sigma}\frac{1}{2}\left\{\left(A_{n\sigma}^{(1)} + B_{n\sigma}^{(2)}\right)\cos(\sigma t - nz) + \left(B_{n\sigma}^{(1)} - A_{n\sigma}^{(2)}\right)\sin(\sigma t - nz)\right\} \\ &+ \sum_{n,\sigma}\frac{1}{2}\left\{\left(A_{n\sigma}^{(1)} - B_{n\sigma}^{(2)}\right)\cos(\sigma t + nz) + \left(B_{n\sigma}^{(1)} + A_{n\sigma}^{(2)}\right)\sin(\sigma t + nz)\right\}\,.\end{aligned} \tag{3}$$

The first term in (3) represents the contributions from all the waves with upward phase velocities, and the second term comes from the contributions of all the waves with downward phase velocities. Thus, the original oscillation profile $\psi(z,t)$ can be divided into a phase-upward profile $U(z,t)$ and a phase-downward profile $D(z,t)$:

$$U(z,t) = \sum_{n,\sigma} \frac{1}{2} \left\{ \left(A_{n\sigma}^{(1)} + B_{n\sigma}^{(2)} \right) \cos(\sigma t - nz) + \left(B_{n\sigma}^{(1)} - A_{n\sigma}^{(2)} \right) \sin(\sigma t - nz) \right\} , \tag{4a}$$

$$D(z,t) = \sum_{n,\sigma} \frac{1}{2} \left\{ \left(A_{n\sigma}^{(1)} - B_{n\sigma}^{(2)} \right) \cos(\sigma t + nz) + \left(B_{n\sigma}^{(1)} + A_{n\sigma}^{(2)} \right) \sin(\sigma t + nz) \right\} . \tag{4b}$$

Notice that the summations are made over selected frequency windows and wave number windows, case by case. We shall analyze $U(z,t)$ and $D(z,t)$ instead of the original data set $\psi(z,t)$.

III-2. Method of phase and group velocity tracing

An RTI plot of the local power of $\Phi(z,t)$ (representing either $U(z,t)$ or $D(z,t)$) can be obtained by the following procedure [15]: At each time step $t_i = i\Delta t$ and height $z_k = k\Delta z$, a time series of N data points (N is chosen to be 15 in this paper) is defined by

$$\{\Phi_{lk} = \Phi(z_k, t_l), \quad l = i - \frac{N}{2}, i - \frac{N}{2} + 1, \ldots, i + \frac{N}{2}\}. \tag{Set 1}$$

First, to remove a very long period wave contribution, a linear trend of this time series (Set 1), $y = at + b$, is obtained by the method of least squares fitting, then a new time series (Set 2) is obtained from (Set 1) by subtracting its linear trend:

$$\{\Phi'_{lk} = \Phi_{lk} - at_l - b, \quad l = i - \frac{N}{2}, i - \frac{N}{2} + 1, \ldots, i + \frac{N}{2}\}. \tag{Set 2}$$

Then, the time series (Set 2) is Fourier analyzed to obtain the power P_{ki} of the first harmonic. Considering P_{ki} as an index of the strength of the wave activity at height z_k and time t_i, we plot the matrix $[P_{ki}]$ as an RTI plot for investigation (We use a contour plot to represent the RTI plot in this paper). A numerical simulation study [15] showed that when a wave packet is propagating packets with high regularity would exist in the RTI plot. It was shown that the same phase points of the characteristic wave component of the wave packet form a straight line called the phase trajectory, while the centers of the neighboring packets form another straight line called the energy trajectory. It was also noted that the former determines the direction of the phase progression and the latter constitutes the direction of energy propagation. Therefore the slope of the phase trajectory is just the phase velocity and the slope of the energy trajectory is the group velocity of the wave packet. Also, the horizontal distance between two consecutive packets (corresponding to the peaks and the dips in the oscillation profile) equals one half of the period of the characteristic wave component of the packet.

III-3. Estimation of horizontal wave-vector component along the background wind

A linear gravity wave packet offers a possibility to estimate its horizontal wavelength. Let us start with the gravity wave dispersion relation [17] neglecting the earth-rotation and Eckart's coefficient,

$$n^2 \simeq k_h^2 \left(\frac{\omega_b^2}{\omega^2} - 1 \right) + \frac{k_h}{\omega} u_0'' \,, \tag{5}$$

where

$$\omega = \sigma - k_h u_0 \,. \tag{6}$$

Here ω_b is the Brunt-Vaisala frequency at the location of the observed wave packet; u_0 and u_0'' are the mean flow velocity and its second derivative with respect to height; n is the vertical wave number and k_h is the horizontal wave number along the direction of the background wind velocity; ω and σ are the intrinsic and observed frequencies, respectively. The radar can only measure/observe the frequency σ over a fixed location. As (6) shows, the two frequencies ω and σ are different when the wave propagates in a non-zero wind field. We need to use the Doppler shifted frequency ω in our analysis. The vertical component of the phase velocity v_{pz} and group velocity v_{gz} of the wave packet are obtained from (5) and (6) as follows:

$$v_{pz} = \sigma / n \,, \tag{7}$$

$$v_{gz} = \frac{\partial \sigma}{\partial n} = \frac{\partial \sigma}{\partial \omega} \frac{\partial \omega}{\partial n} = \frac{\partial \omega}{\partial n} = - \left(\frac{\omega_b^2 k_h^2}{n \omega^3} + \frac{k_h u_0''}{2 \omega^2 n} \right)^{-1} \,, \tag{8}$$

where we have applied the fact that $\partial \sigma / \partial \omega = 1$ from (6). After some algebra manipulations of Eqs. (6), (7), and (8), we obtain the equation for the horizontal wave-vector component k_h along the direction of the mean wind velocity:

$$k_h^3 + a k_h^2 + b k_h + c = 0 \,, \tag{9}$$

where the coefficients $a = \frac{u_0 u_0'' v_{gz} - 2 v_{gz} \omega_b^2 - 6 n \sigma u_0^2}{2 n u_0^3}$, $b = \frac{6 n u_0 \sigma^2 - \sigma u_0'' v_{gz}}{2 n u_0^3}$, and $c = -\frac{\sigma^3}{u_0^3}$ are to be determined from the measurable quantities σ, u_0, u_0'', ω_b, v_{pz}, and v_{gz}. We take the value of $\omega_b = 0.0122$ s^{-1} and neglect the effect of u_0'' throughout this analysis.

Note that Eq. (9) has at least one real root. If Eq. (9) has only one real root then it is definitely the solution; it may have three real roots, then we have to set a criterion to decide the solution for k_h. However, the absolute majority (more than 99.9%) of our cases under analysis have only one real root, therefore, we simply discard these very few cases with three real roots without affecting the statistics of the results of our analysis, since these may just result from statistical uncertainties.

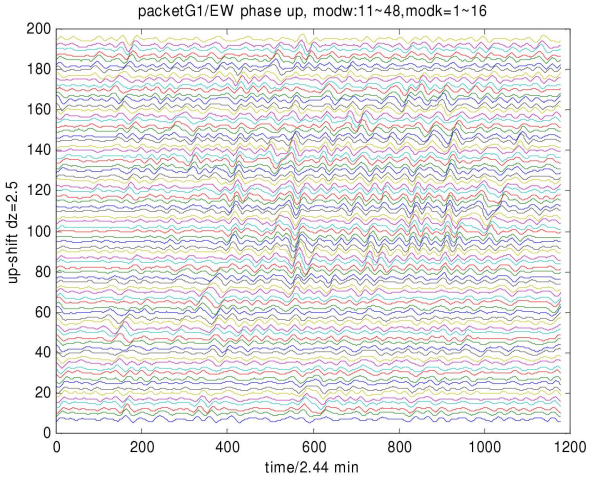

FIG. 1: Oscillation profiles of the phase-upward subset $U(z,t)$ obtained from data set G1. The time resolution is 2.44 min and height resolution is 150 m. The velocity of each height is up-shifted by 2.5 m/s for each subsequent height.

Although a well known phenomenon, for the convenience of discussion it is worth describing how the Doppler shift effect comes about. Since the term involving u_0'' is negligible in many cases, we may rewrite Eq. (8) as

$$v_{gz} = -\left(\frac{\omega_b^2 k_h^2}{n\omega^3} + \frac{k_h u_0''}{2\omega^2 n}\right)^{-1} \simeq -\frac{n\omega^3}{\omega_b^2 k_h^2} = -\frac{\omega}{n}\left(\frac{n\omega}{\omega_b k_h}\right)^2 . \tag{10}$$

Combining Eqs. (7) and (10) we obtain

$$v_{pz} \times v_{gz} = -\frac{\sigma}{n}\frac{\omega}{n}\left(\frac{n\omega}{\omega_b k_h}\right)^2 = -\frac{\sigma}{k_h}\frac{\omega}{k_h}\left(\frac{\omega}{\omega_b}\right)^2 . \tag{11}$$

Eqs. (6) and (11) imply that if the horizontal phase velocity of a wave packet σ/k_h (along the direction of the background wind velocity u_0) is within the range $0 < \sigma/k_h < u_0$, the vertical component of its group velocity v_{gz} will be in the same direction as the vertical component of its phase velocity v_{pz}. This phenomenon has been regarded as a Doppler shift effect.

III-4. Estimation of the angle between the horizontal wave-vector and background wind

We start from the polarization equation [17],

$$\frac{\tilde{U}}{\tilde{V}} = \frac{\omega k + i2\Omega_z l}{\omega l - i2\Omega_z k} , \tag{12}$$

where $i = \sqrt{-1}$; $\tilde{U}$ and $\tilde{V}$ are, respectively, the amplitude of the zonal and meridional component of the fluctuation wind velocity; k and l are the eastward and northward component of the wave vector; ω (see Eq. (6)) is the characteristic intrinsic frequency of the wave packet, while $2\Omega_z$ (= 0.000142 s^{-1}) is the inertial frequency above the fixed radar site. We define $\beta = |\tilde{U}/\tilde{V}|$, $\alpha = \omega/2\Omega_z$, and $\gamma = k/l$, then Eq. (12) reduces to

$$\beta = \left| \frac{\alpha \cdot \gamma + i \cdot 1}{\alpha - i \cdot \gamma} \right| = \frac{\sqrt{\alpha^2\gamma^2 + 1}}{\sqrt{\alpha^2 + \gamma^2}}, \tag{13}$$

or inversely,

$$\frac{k}{l} = \gamma = \pm\sqrt{\frac{\alpha^2\beta^2 - 1}{\alpha^2 - \beta^2}}. \tag{14}$$

Note that Eq. (14) is valid if and only if $(\alpha^2\beta^2 - 1)/(\alpha^2 - \beta^2) \geq 0$. We refer to an event with $(\alpha^2\beta^2 - 1)/(\alpha^2 - \beta^2) \geq 0$ as a valid event and call it an invalid event otherwise.

The angle θ between the horizontal wave vector $\vec{K} = k\hat{x} + l\hat{y}$ and the background wind velocity $\vec{U}_0 = u_{0x}\hat{x} + u_{0y}\hat{y}$ is given by

$$\cos\theta = \frac{\vec{K} \cdot \vec{U}_0}{|\vec{K}| \cdot |\vec{U}_0|} = \frac{k \cdot u_{0x} + l \cdot u_{0y}}{\sqrt{k^2 + l^2} \cdot \sqrt{u_{0x}^2 + u_{0y}^2}} = \frac{\gamma \cdot u_{0x} + u_{0y}}{\sqrt{\gamma^2 + 1} \cdot \sqrt{u_{0x}^2 + u_{0y}^2}} = \delta. \tag{15}$$

Since Eq. (14) provides either a positive or negative value for k/l $(= \gamma)$, there exist two possible values for $\cos\theta$ given by Eq. (15). Unfortunately, we are unable, with the applied computational method, to decide which one is the true value for each event and must thus take both values into consideration in our statistical analysis. Furthermore, the true value of θ can be either $\cos^{-1}\delta$ or $180^\circ - \cos^{-1}\delta$, we must distinguish one from the other in practical data analysis. In future analyses we will try to deduce the full information on the wave propagation by tracing the wave oscillations in the five different beam directions.

IV. ANALYSIS OF THE SOUSY-SVALBARD DATA

Five data sets with each set lasting for 2 days were selected for horizontal wave vector analysis. The observation dates of each data set are listed in Table I. The time resolution is 2.44 minutes and the height resolution is 150 meters for each set. The frequency window to be summarized in Eqs. (4a) and (4b) is 4.0×10^{-4} $s^{-1} < \sigma < 1.82 \times 10^{-3}$ s^{-1} (corresponding to the wave periods 261.3 min$> \tau >$57.5 min) and the wave number window is 5.23×10^{-4} $m^{-1} < n < 8.37 \times 10^{-3}$ m^{-1} (corresponding to vertical wavelengths 12 km$> \lambda >$0.75 km). Since the rest of the processes of wave analysis for all the data sets are identical, we will describe the analysis process of one data set as an example. The vertical velocity $\psi(z,t)$ of the data set coded by G1 is divided into two subsets, a phase-upward subset $U(z,t)$ (as shown in Fig. 1) and phase-downward subset $D(z,t)$ (not shown). Part of the RTI plot

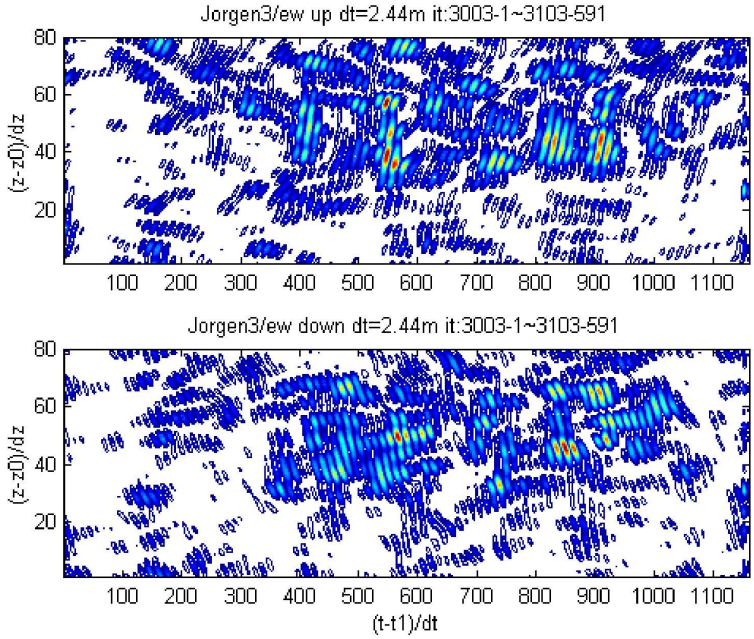

FIG. 2: The RTI plots deduced from the oscillation profiles of data set G1. The upper panel is deduced from the phase upward subset $U(z,t)$ (shown in Fig. 1) and the lower panel is deduced from the phase downward subset $D(z,t)$, with $N = 15$ and time resolution $dt = 2.44$ min. A frequency window of 4.0×10^{-4} s^{-1}< σ < 1.82×10^{-3} s^{-1} (corresponding to the wave periods 261.3 min> τ >57.5 min) and wave number window of 5.23×10^{-4} m^{-1}< n < 8.37×10^{-3} m^{-1} (corresponding to vertical wavelengths 12 km> λ >0.75 km) were used in this analysis.

converted from the subsets $U(z,t)$ by the method of phase and group velocity tracing is shown in the upper panel of Fig. 2, while that from the subset $D(z,t)$ is shown in the lower panel. Each packet in the upper panel of Fig. 2 reveals a positive slope implying an upward phase velocity; and each packet in the lower panel reveals a negative slope implying a downward phase velocity, as expected. The group velocity of a wave-packet can be obtained from the slope of its energy line, which is the line connecting the central points of the neighboring packets. It is easy to decide the group velocity direction of each wave packet just by eye-ball inspection. The RTI plots in Fig. 2 reveal that the group and phase velocities of most of the wave packets have an opposite sense of vertical propagation (referred as Type 1 wave packets); the group and phase velocities of some wave packets have the same sense of vertical propagation (referred as Type 2 wave packets). From the linear theory of the gravity wave dispersion relation as described in the previous section, a gravity wave packet will appear as Type 2 only if its characteristic horizontal phase velocity σ/k_h (along the background wind direction) is in the range $0 < \sigma/k_h < u_0$. Otherwise, it will appear as Type 1 if $\sigma/k_h < 0$ or $u_0 < \sigma/k_h$ (Note: σ and u_0 are always positive).

TABLE I: The first and last dates of each data set of Group 1. The starting time of each set is 00:00 and the end time is 23:59.

Data Set	Start date	End date	# of good Type 1 packet elements	# of good Type 2 packet elements
G1	March 30	March 31	229	60
H1	April 1	April 2	97	21
M1	April 11	April 12	195	71
Q1	April 21	April 22	165	61
R1	April 23	April 24	183	55
Total #			869	268

An element of a wave packet defined by three consecutive patches is the basic unit for group and phase velocity measurement. Fig. 3 shows an example of a velocity measurement taken from the data set G1. The slope of the phase line along the middle patch equals the vertical phase velocity, while the slope of the energy line across the three patches equals the vertical group velocity. This specific example is a Type 1 wave packet. Any specific element of a wave packet is confined in the box bounded by $z_1 < z < z_2$ in the height domain and $t_1 < t < t_2$ in the time domain, and these boundaries (z_1, z_2, t_1, t_2) are decided at the velocity measurement. An example of a box of the same wave packet event of Fig. 3 is demonstrated in Fig. 4. We estimate the corresponding wave amplitude $(\tilde{U}, \tilde{V})$ and the background wind velocity (u_{0x}, u_{0y}) within the boundaries of the wave packet element as follows:

$$\tilde{U} = \frac{1}{\tilde{N}} \sqrt{\sum_{t=t_1}^{t_2} \sum_{z=z_1}^{z_2} \tilde{u}^2(t,z)}\,, \tag{16a}$$

$$\tilde{V} = \frac{1}{\tilde{N}} \sqrt{\sum_{t=t_1}^{t_2} \sum_{z=z_1}^{z_2} \tilde{v}^2(t,z)}\,, \tag{16b}$$

$$u_{0x} = \frac{1}{\tilde{N}} \sum_{t=t_1}^{t_2} \sum_{z=z_1}^{z_2} u(t,z)\,, \tag{17a}$$

$$u_{0y} = \frac{1}{\tilde{N}} \sum_{t=t_1}^{t_2} \sum_{z=z_1}^{z_2} v(t,z)\,, \tag{17b}$$

where $\tilde{u}(t,z)$ and $\tilde{v}(t,z)$ are the zonal and meridional component of the fluctuation velocity at the time t and height z, respectively, while $u(t,z)$ and $v(t,z)$ are, respectively, the zonal and meridional component of the horizontal wind velocity at the time t and height z. $\tilde{N}$

is the total number of available data points within the given boundaries. There are some missing data points in the data set due to insufficient signal power or time breaks during the experiment operation. Before doing a wave packet analysis (see section III-2), these gaps due to missing data were synthetically filled by zeros. This action will cause some error in the group and phase velocity measurement, the higher the percentage of missing data, the larger the error will be. A wave packet element is said to be a good event, if its missing data is less than 10% of its total data points within its boundary. And the missing data is not taken into account in calculating $(\tilde{U}, \tilde{V})$ and (u_{0x}, u_{0y}). It is required that at least 50% of the wave packet events measured in a data set are good events to be accepted for further statistical analysis. The numbers of good events of each acceptable data set are listed in Table I. This reveals that the ratio between Type 1 wave packet events and Type 2 events is 3.24 : 1.

For each good event (good wave packet element), the vertical phase velocity v_{pz} and group velocity v_{gz} are obtained from the slopes of the phase line and energy line, respectively, as in the example shown in Fig. 3, the corresponding wave amplitude $(\tilde{U}, \tilde{V})$ and the background wind velocity (u_{0x}, u_{0y}) within the box, as in the example shown in Fig. 4, are calculated from Eqs. (16) and (17), respectively. Then the horizontal wave vector component k_h along the direction of the mean wind velocity is obtained by Eq. (9), and consequently the horizontal wavelength $\lambda_h = 2\pi/k_h$ along the direction of mean wind velocity is obtained. The angle $|\theta|$ between the horizontal wave vector $\vec{K} = k\hat{z} + l\hat{y}$ and the background wind velocity $\vec{U}_0 = u_{0x}\hat{x} + u_{0y}\hat{y}$ is estimated from Eqs. (13)–(15). We have analyzed in such a manner a total of 1137 good wave packet elements, as can be seen from Table I.

The statistics (mean ± standard deviation) of the measured vertical phase velocity v_{pz}, group velocity v_{gz}, characteristic wave period τ, the deduced horizontal wavelength λ_h along the direction of horizontal mean wind, and the ratio $\Re$, are summarized in Table II and III. Here $\Re$ is defined as the ratio between the horizontal phase velocity $v_{ph} = \lambda_h/\tau$ along the direction of horizontal mean wind velocity and the mean wind speed, i.e., $\Re = v_{ph}/\sqrt{u_{0x}^2 + v_{0y}^2}$. The good wave packet events are divided into four subsets for this statistical analysis: namely, the Type 1 events with upward group velocities are summarized in Table IIa, while Type 1 events with downward group velocities are in Table IIb; the Type 2 events with upward group velocities are summarized in Table IIIa, while Type 2 events with downward group velocities are in Table IIIb. Comparing Table IIa with IIb of Type 1 wave packets, and also comparing Table IIIa with IIIb of Type 2 wave packets, it can be seen that the statistics of wave packets with positive v_{gz} are similar with those of the wave packets with negative v_{gz} of the same type events. Basically, the characteristic wave periods of the wave packets picked by the predefined window are approximately 70 minutes, with rather small fluctuations. On the contrary, the ranges of the corresponding horizontal wave lengths λ_h along the direction of the mean wind velocity are relatively large: the range of λ_h is 20–80 km for Type 1 packets, and 10–45 km for Type 2 packets. The characteristic horizontal phase velocities v_{ph} of most Type 1 packets along the direction of the mean wind are larger than the mean wind speed ($\Re > 1$), and that of most Type 2 packets are smaller

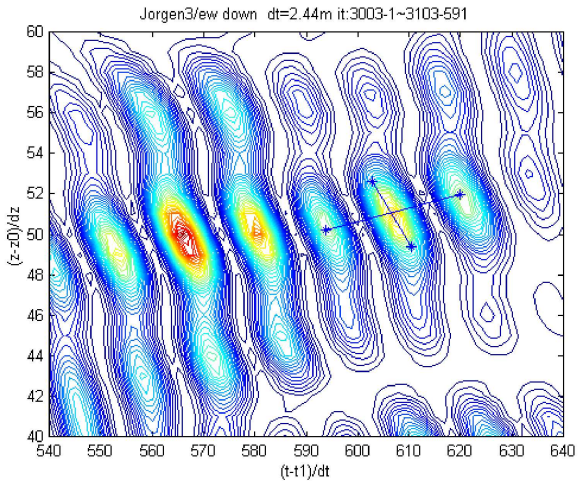

FIG. 3: Demonstration of vertical phase and group velocity measurement of a wave packet element. The slope of the phase line along the central patch equals the phase velocity, while that of the energy line connecting the centers of the three consecutive patches equals the group velocity of the wave packet.

than the mean wind speed ($\Re < 1$), as the statistics of the velocity ratio $\Re$ shows. This is consistent with the prediction of linear gravity wave theory.

We have carefully checked the solution of Eq. (9) for each wave packet event, and found that no event has a negative k_h solution. That means no wave packet is found to move against the background wind. This interesting result deserves more discussion. We note that if a wave propagates against the background wind its k_h must be negative, then its intrinsic frequency ω will be larger than the observed frequency σ, as Eq. (6) reveals (both σ and u_0 in Eq. (6) are positive). Consequently, such a wave packet will move much faster than the wave packets with positive k_h, as Eq. (10) shows that $v_{gz} \propto \omega^3$. A faster moving target will receive less exposure time at the same spot than a slower moving target. This makes a wave packet with negative k_h harder to be detected by radar. So we must emphasize that failing to detect a wave packet moving against the wind doesn't mean that it doesn't exist at all. According to linear gravity wave theory, a Type 1 wave packet (with $k_h > 0$) should have a speed ratio $\Re$ larger than 1, while a Type 2 wave packets (also with $k_h > 0$) should have $\Re$ smaller than 1 due to the Doppler shift effect. Let's call an event satisfying linear gravity wave theory a normal event and an abnormal event otherwise. We found 36 out of 869 Type 1 wave packets (4.14%) are abnormal, while all the Type 2 wave packets are found to be normal events. Considering the existence of missing data and false human assessments in measuring the slopes of phase and energy lines, the percentage of abnormal events seems to be acceptable.

Another parameter of the horizontal wave vector $\vec{K} = k\hat{x} + l\hat{y}$ is its angle θ with respect to the background wind velocity $\vec{U}_0 = u_{0x}\hat{x} + u_{0y}\hat{y}$. Since the solution k_h of Eq. (9)

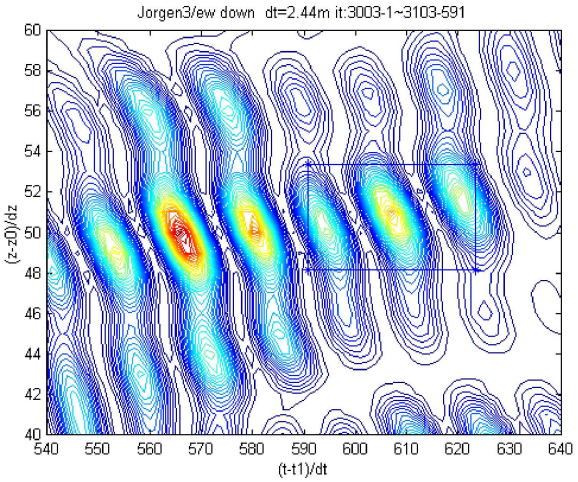

FIG. 4: Demonstration of the boundaries of a box confining the wave packet element to be measured. The horizontal wave amplitudes and the background wind velocity seen by this wave packet are to be calculated within this box by Eqs. (14) and (15), respectively.

TABLE II: (a) Statistics (mean ± standard deviation) of the measured vertical phase velocity v_{pz}, group velocity v_{gz}, characteristic wave period τ, the deducted horizontal wavelength λ_h along the direction of horizontal mean wind, and the ratio $\Re$, for Type 1 wave packets with upward group velocity.

Data Set	v_{pz}(m/s)	v_{gz}(m/s)	τ(min)	λ_h(km)	$\Re$
G1	-0.60 ± 0.19	0.071 ± 0.057	68.7 ± 5.81	48.7 ± 14.6	1.37 ± 0.15
H1	-0.54 ± 0.29	0.088 ± 0.069	68.2 ± 4.05	32.4 ± 10.8	1.56 ± 0.26
M1	-0.53 ± 0.18	0.091 ± 0.086	69.7 ± 4.90	49.1 ± 17.3	1.40 ± 0.19
Q1	-0.38 ± 0.12	0.096 ± 0.064	71.6 ± 6.07	64.8 ± 21.5	1.23 ± 0.21
R1	-0.39 ± 0.11	0.069 ± 0.055	69.2 ± 4.44	41.1 ± 14.4	1.38 ± 0.20

TABLE II: (b) Statistics (mean ± standard deviation) of the measured vertical phase velocity v_{pz}, group velocity v_{gz}, characteristic wave period τ, the deducted horizontal wavelength λ_h along the direction of horizontal mean wind, and the ratio $\Re$, for Type 1 wave packets with downward group velocity.

Data Set	v_{pz}(m/s)	v_{gz}(m/s)	τ(min)	λ_h(km)	$\Re$
G1	0.56 ± 0.23	-0.088 ± 0.068	68.7 ± 6.33	50.3 ± 13.2	1.38 ± 0.15
H1	0.52 ± 0.16	-0.107 ± 0.066	67.2 ± 4.03	36.3 ± 9.23	1.51 ± 0.18
M1	0.58 ± 0.29	-0.070 ± 0.054	68.0 ± 4.63	44.6 ± 16.4	1.38 ± 0.19
Q1	0.39 ± 0.10	-0.082 ± 0.053	69.9 ± 6.76	59.3 ± 19.4	1.25 ± 0.17
R1	0.44 ± 0.14	-0.063 ± 0.051	69.8 ± 5.32	36.4 ± 15.6	1.42 ± 0.20

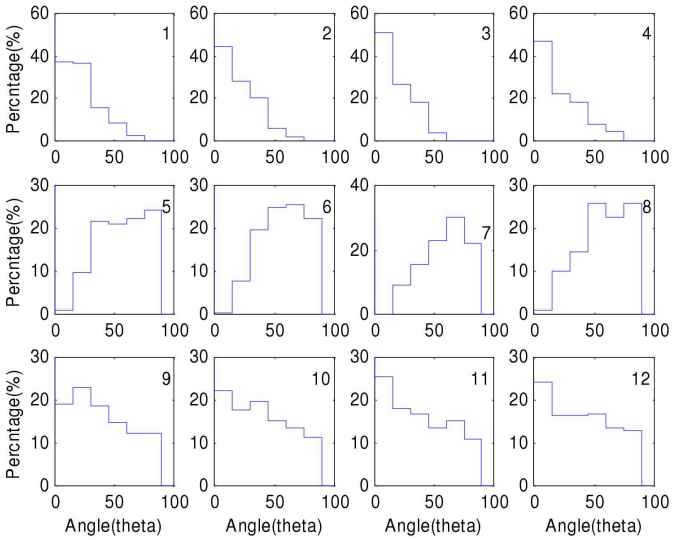

FIG. 5: θ-distributions for different subgroups of wave packets. From top to bottom, the diagrams in the first row (diagram 1–4) are the θ_S distributions for different subgroups of wave packet events, the diagrams in the second row (diagram 5–8) are the θ_L distributions for the corresponding subgroups of wave packets; the average between the corresponding distributions in the first row and the second row are shown in the third row (diagram 9–12). From left to right, the diagrams are the distributions for the Type 1 wave packets with $v_{gz} > 0$ (first column), Type 1 wave packets with $v_{gz} < 0$ (second column), Type 2 wave packets with $v_{gz} > 0$ (third column), and Type 2 wave packets with $v_{gz} < 0$ (fourth column). The definitions of θ_S and θ_L are given in the text.

for each packet event is unanimously found to be positive, the angle θ should be in the range $-90^\circ \sim 90^\circ$. Also there is no significant physical meaning in distinguishing positive θ from negative θ; we shall always consider θ as positive for simplicity, i.e., $0^\circ \leq \theta \leq 90^\circ$. We apply Eqs. (13)–(15) to calculate $\cos\theta$ for each wave packet event. First of all, the invalid events with $(\alpha^2\beta^2 - 1)/(\alpha^2 - \beta^2) < 0$ (see Eq. (14)) must be removed from analysis. We found that 153 out of 869 (17.6%) Type 1 wave packets and 57 out of 268 (21.3%) Type 2 wave packets are invalid. For those valid events there exist two possible values for γ $(= k/l)$ given by Eq. (14), for the convenience of discussion we define $\theta = \theta_+$ and $\delta = \delta_+$ in the case of $\gamma = \gamma_+ > 0$, $\theta = \theta_-$ and $\delta = \delta_-$ when $\gamma = \gamma_- < 0$ in Eq. (15). Then from Eq. (15) we have $\theta_+ = \cos^{-1}\delta_+$ or $180^\circ - \cos^{-1}\delta_+$ ($\theta_- = \cos^{-1}\delta_-$ or $180^\circ - \cos^{-1}\delta_-$), whichever is in the range of 0°–90°. Unfortunately, there is no further information to tell us which one of θ_+ and θ_- is the true value, so a further assumption is needed to make a statistical analysis. We will in a further analysis try to also determine this information from the five-beam observations. If the smaller angle is true, we should take $\theta_S = \min\{\theta_+, \theta_-\}$ as the final solution of θ, otherwise, we should take $\theta_L = \max\{\theta_+, \theta_-\}$ as the final solution. Since we do

TABLE III: (a) Statistics (mean ± standard deviation) of the measured vertical phase velocity v_{pz}, group velocity v_{gz}, characteristic wave period τ, the deducted horizontal wavelength λ_h along the direction of horizontal mean wind, and the ratio $\Re$, for Type 2 wave packets with upward group velocity.

Data Set	v_{pz}(m/s)	v_{gz}(m/s)	τ(min)	λ_h(km)	$\Re$
G1	0.60 ± 0.31	0.032 ± 0.025	70.1 ± 6.73	28.1 ± 8.28	0.78 ± 0.07
H1	0.60 ± 0.24	0.035 ± 0.017	67.5 ± 2.40	14.8 ± 6.97	0.68 ± 0.10
M1	0.67 ± 0.24	0.035 ± 0.024	66.2 ± 4.41	24.2 ± 12.0	0.75 ± 0.08
Q1	0.45 ± 0.14	0.031 ± 0.022	69.2 ± 6.12	32.1 ± 13.7	0.80 ± 0.07
R1	0.43 ± 0.12	0.029 ± 0.022	67.3 ± 5.21	19.5 ± 13.5	0.71 ± 0.16

TABLE III: (b) Statistics (mean ± standard deviation) of the measured vertical phase velocity v_{pz}, group velocity v_{gz}, characteristic wave period τ, the deducted horizontal wavelength λ_h along the direction of horizontal mean wind, and the ratio $\Re$, for Type 2 wave packets with downward group velocity.

Data Set	v_{pz}(m/s)	v_{gz}(m/s)	τ(min)	λ_h(km)	$\Re$
G1	-0.62 ± 0.19	-0.023 ± 0.018	66.6 ± 3.43	26.9 ± 8.56	0.80 ± 0.08
H1	-0.46 ± 0.07	-0.036 ± 0.036	72.9 ± 10.2	26.1 ± 16.5	0.75 ± 0.13
M1	-0.55 ± 0.22	-0.034 ± 0.025	70.3 ± 5.39	23.7 ± 8.25	0.76 ± 0.08
Q1	-0.43 ± 0.19	-0.028 ± 0.026	69.9 ± 5.06	44.5 ± 20.4	0.83 ± 0.06
R1	-0.44 ± 0.12	-0.032 ± 0.021	68.6 ± 4.16	22.2 ± 12.3	0.74 ± 0.12

not know which one is true, we shall study the statistics of θ_S and θ_L instead of the true θ. Fig. 5 shows the angle distributions of different subgroups of wave packet events. There are 12 diagrams in three rows and four columns: From top to bottom, the diagrams in the first row (diagram 1–4) are the θ_S-distributions for different subgroups of wave packet events, the diagrams in the second row (diagram 5–8) are the θ_L-distributions of the corresponding subgroups of wave packets; the average between the corresponding distributions in the first row and the second row are shown in the third row (diagram 9–12). From left to right, the diagrams are the distributions for the Type 1 wave packets with $v_{gz} > 0$ (first column), the Type 1 wave packets with $v_{gz} < 0$ (second column), the Type 2 wave packets with $v_{gz} > 0$ (third column), and the Type 2 wave packets with $v_{gz} < 0$ (fourth column), respectively. The distributions in the third row unanimously show that the percentages of wave packets are monotonically decreasing with angle, this seems to imply that the smaller angle θ_S is more likely to be true than the larger angle θ_L.

V. SUMMARY AND DISCUSSION

In this study phase and group velocity tracing [15] was proved to be an efficient method to measure the vertical phase and group velocity of wave propagation in the atmo-

sphere. It offers information on the characteristic wave period and the vertical wavelength of the wave packet. It also allows one to estimate the horizontal wave vector component k_h along the direction of the mean wind velocity by applying the dispersion relation, and the angle between the horizontal wave vector and the mean wind velocity by the polarization equation. We have analyzed the wave packets of five data sets with characteristic periods of ~70 minutes with small fluctuations. The events are selected by a predefined frequency window of 4.0×10^{-4} s^{-1}< σ < 1.82×10^{-3} s^{-1} (corresponding to the wave periods 261.3 min> τ >57.5 min). It is clear that the characteristic wave periods of the wave packets tend to approach the high frequency end of the window. This is true because the relative frequency resolution $\Delta\sigma/\sigma$ is better for higher frequency wave components (note that $\Delta\sigma$ is same for each component wave in the packet).

There are two types of wave packets observed in this study: Type 1 with phase and group velocities having the opposite sense of vertical propagation, and Type 2 having the same sense of vertical propagation. The number of Type 1 events is found to be 3.24 times that of Type 2 events. In a previous paper [16] (Kuo *et al.*, 2003), we reported that the number of Type 1 wave packet events with characteristic wave periods in the range 15–45 minutes is about 5.67 times that of Type 2 events. The probability of the occurrence of Type 2 wave packets seems to increase with the wave period, but more analyses of wave packets with different characteristic periods are needed to confirm this speculation. An important point is that the percentage of Type 2 wave packets is so significant that it should be taken into consideration as far as energy transport is concerned. Traditionally, one tends to regard the opposite direction of the vertical phase velocity as the direction of energy transport by atmospheric gravity waves. Results of this study indicate that such a conventional way of thinking should be changed. The energy propagation of gravity waves in the vertical direction should be decided by measuring their group velocities directly, for instance by applying the method presented here.

The horizontal wave vector component k_h along the direction of the background wind velocity can be calculated by Eq. (9) only when both vertical phase and group velocities as well as the background wind velocity are available. The sign of k_h has an important physical meaning: if k_h is positive the gravity wave propagates along its background wind, otherwise it propagates against the background wind. Among a total number of 1137 good wave packets we have not found any wave packet to move against the background wind. The angle θ between the horizontal wave vector and the background wind velocity can be obtained from Eqs. (13)–(15). If k_h is positive $|\theta|$ will be in the range 0°–90°, if k_h is negative $|\theta|$ will be in the range 90°–180°. Statistical analysis on θ among the wave packet events reveals that the number of wave packets decreases with $|\theta|$ increasing from 0° to 90°. This may help explain why there are very few wave packets (if any exist) moving against the background wind.

Finally we must make a remark on the dispersion relation (5), in which we have neglected the earth rotation. This approximation is valid for high frequency waves (i.e., $\omega >> 2\Omega_z$). For the cases in this study, the average wave period is $\tau \simeq 70$ min (see Table IIa and IIb), corresponding to an average wave frequency of $\sigma \simeq 1.5 \times 10^{-3}$ s^{-1}. Considering the fact that the mean value of the velocity ratio for a Type 1 packet is $\Re \simeq 1.4$ (see

Table IIa and IIb), the average intrinsic frequency is $\omega \simeq 0.29\sigma \simeq 4.35 \times 10^{-4}$. The inertial frequency at the radar site is $2\Omega_z = 1.42 \times 10^{-4}$ s^{-1} and the Brunt-Vaisala frequency is $\omega_b = 0.0122$ s^{-1}. When these numbers are put into the dispersion relation with the inertial frequency included,

$$n^2 \simeq k_h^2 \left(\frac{\omega_b^2 - \omega^2}{\omega^2 - 4\Omega_z^2} \right) \Rightarrow \quad n \simeq 29.65 k_h \,. \tag{18}$$

If the earth rotation is neglected, i.e., let $2\Omega_z = 0$, then $n \simeq 28.03 k_h$. The effect of neglecting the earth rotation on the vertical wave number n is about 5.5%. For Type 2 wave packets, $\tau \simeq 70$ min, $\sigma \simeq 1.5 \times 10^{-3}$ s^{-1}, and $\Re \simeq 0.8$ (see Table IIIa and IIIb), these data lead to $\omega \simeq -0.25\sigma \simeq -3.75 \times 10^{-4}$ s. Then $n \simeq 35.1 k_h$ if the inertial frequency is included, and $n \simeq 32.5 k_h$ if the inertial frequency is neglected. The effect of $2\Omega_z$ on n is about 7.4%.

Acknowledgments

This work is supported in part by the National Science Council of Taiwan under the contract number NSC 92-2111-M-238-001. The second author (JR) would like to thank his colleagues at the National Central University for their hospitality during his stay as visiting professor, which was possible through the National Science Council grant NSC90-2811-M-008-013. The SOUSY Svalbard Radar was a project of the Max-Planck-Institute and is now operated under the Tromsø Geophysical Observatory of the University in Tromsø. We thank all involved colleagues for their assistance in taking the data.

References

[1] T. E. VanZandt, J. L. Green, W. L. Clark, and J. R. Grant, Geophys. Res. Lett. **6**, 429 (1979).
[2] S. Fukao, K. Wakasuki, and S. Kato, Radio Sci. **15**, 447 (1980).
[3] W. L. Ecklund, K. S. Gage, and A. C. Riddle, Geophys. Res. Lett. **8**, 285 (1981).
[4] G. D. Nastrom, M. R. Peterson, J. L. Green, K. S. Gage, and T. E. Vanzandt, Jour. Appl. Met. **25**, 783 (1990).
[5] W. L. Ecklund, K. S. Gage, G. D. Nastrom, and B. B. Balsley, Jour. Climate Appl. Met. **25**, 885 (1986).
[6] R. Vincent, and I. M. Reid, Jour. Atmosph. Sci. **40**, 1321 (1983).
[7] I. M. Reid, and R. A. Vincent, J. Atmos. Terr. Phys. **49**, 443 (1987).
[8] R. M. Worhington, and L. Thomas, Radio Sci. **31**, 1501 (1996).
[9] D. C. Fritts, J. F. Garten, D. M. Riggin, R. A. Goldberg, G. A. Lehmacher, F. J. Schmidlin, S. McCarthy, E. Kudeki, C. D. Fawcett, M. H. Hitchman, R. S. Lieberman, I. M. Reid, and R. A. Vincent, J. Geophys. Res. **102**, 26191 (1997).
[10] D. M. Riggin, D. C. Fritts, C. D. Fawcett, E. Kudeki, and M. H. Hitchman, J. Geophys. Res. **102**, 26263 (1997).
[11] D. C. Fritts, and L. Yuan, J. Atmos. Sci. **46**, 2569 (1989).
[12] K. Sato, and M. Yamada, J. Geophys. Res. **99**, 10623 (1994).
[13] J. Röttger, Advances in Polar Upper Atmosphere Research **14**, 202 (2001).

[14] C. O. Hines, Can. J. Phys. **38**, 1441 (1960).
[15] F. S. Kuo, H. Y. Lue, and C. L. Luo, J. Atmos. Solar Terr. Phys. **60**, 455 (1998).
[16] F. S. Kuo, J. Röttger, and H. Y. Lue, Chinese Journal of Physics **41**, 309 (2003).
[17] E. E. Gossard and W. H. Hooke, *Waves in the Atmosphere* (Elsevier, New York, 1975).